

## Supporting Information

### Experimental and Computational Insights into CuS-Mg Composites for High-Performance p-Type Transparent Conducting Materials

Stener Lie, Qingde Sun, Pritish Mishra, Patrick Wen Feng Li, Anupam Sadhu, Teddy Salim, Shuzhou Li, Geoffroy Hautier and Lydia Helena Wong\*

#### Experimental Procedures

**CuS-Mg thin film preparation:** The precursor solution was prepared by dissolving copper chloride dihydrate ( $\text{CuCl}_2 \cdot 2\text{H}_2\text{O}$ ), magnesium chloride hexahydrate ( $\text{MgCl}_2 \cdot 6\text{H}_2\text{O}$ ) and thiourea ( $\text{CH}_4\text{N}_2\text{S}$ ) into D.I. water. The chemical precursors were purchased from Sigma Aldrich with purity of 99.99%. Excess of thiourea ( $\text{SC}(\text{NH}_2)_2$ ) of 0.2 M was added to the solution as sulfur source. The solution was stirred until clear solution was obtained. Before spray coating, soda lime glass substrates were cleaned using Alconox® detergent, ethanol, and isopropyl alcohol (IPA) in ultrasonic bath for 20 minutes each. Following that, UV-ozone treatment was performed for 20 minutes. The precursor solution was sprayed on top of heated glass substrates. The spray parameters are as following: hot plate temperature of 300 °C, gas pressure of 10 Psi, solution flow rate of 0.85 ml/s and spray distance of 25 cm. After spray finished, thin film is slowly cooled. For high-throughput fabrication, an ultrasonic spray nozzle coupled with an XYZ motorized stage was used to enable automated and uniform deposition across multiple samples. The system's syringes fed separate precursor solutions (e.g., Cu and Mg), and their flow rates were independently controlled to achieve precise molar ratios in the deposited films. The system features a  $30 \times 30 \text{ cm}^2$  hotplate, capable of accommodating up to 14–16 substrates ( $2.5 \times 2.5 \text{ cm}^2$  each) in one run. To vary the film thickness, the amount of volume used for spray coating can be adjusted – with 5 ml volume, 180 nm thickness can be obtained. A schematic of the setup is shown below in figure S1.

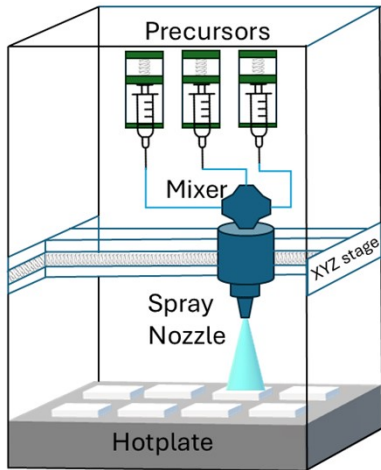


**Fig. S1.** Schematic of high throughput automated spray pyrolysis system

**Heterojunction device fabrication:** The heterojunction devices were fabricated with CuS-Mg/CdS/electrode configuration. The electrode used in this study was Ag metal and FTO. Spray pyrolysis of CdS layer was performed on 300 °C hotplate, gas pressure of 10 Psi, solution flow rate of 0.85 ml/s and spray distance of 25 cm, using 5 ml of 0.005 M CdCl<sub>2</sub> and CH<sub>4</sub>N<sub>2</sub>S 0.2 M on aqueous environment. Following that, either thermally evaporated Ag (0.5 × 0.5 cm<sup>2</sup>) or sputter-deposited fluorine-doped tin oxide (FTO) with a thickness of around 100 nm was prepared on top of CdS to complete the device fabrication.

As for the chemicals for perovskite fabrication, Lead iodide (PbI<sub>2</sub>, 99.99%) and lead bromide (PbBr<sub>2</sub>, >98%), cesium iodide (CsI, 99.999%), chlorobenzene (99.8%), dimethylformamide (DMF, 99.8%), and dimethyl sulfoxide (DMSO, 99.9%) are purchased from Sigma Aldrich. Methylammonium bromide (MABr, >99.99%) and formamidinium iodide (FAI, >99.99%) are purchased from GreatCell Solar. PCBM (99.5%), spiro-OMeTAD (99.5%) are purchased from Lumtec Corp. Poly(3,4-ethylenedioxythiophene)-poly(styrenesulfonate) (PEDOT:PSS PH 1000) is purchased from Ossila. Following the CuS-Mg fabrication, PEDOT:PSS 150 μL is spin-coated on top at 2500 rpm for 60 s and annealed at 120°C for 20 mins inside glovebox. Followed by perovskite layer which is made by having 1.2 M concentration of PbI<sub>2</sub>, PbBr<sub>2</sub>, CsI, MAI and FAI in Dimethylformamide (DMF) and Dimethyl sulfoxide (DMSO) with stoichiometry of Cs<sub>0.05</sub>(MA<sub>0.17</sub>FA<sub>0.83</sub>)<sub>0.95</sub>Pb(I<sub>0.83</sub>Br<sub>0.17</sub>)<sub>3</sub> and DMF: DMSO ratio was 4:1. 30-40 μL of perovskite solution was spin-coated at 2000 rpm for 10 s followed by 6000 rpm for 30 s. 100 μL of chlorobenzene was dripped in 5 seconds before spin ends. Substrates were then annealed at 100°C for 45 min. A 20 mg/ml PCBM solution in chlorobenzene is used to deposit the electron transport layer. PCBM deposition is completed at a spin speed of 2000 rpm for 30

seconds, followed by an annealing step at 90 °C for 10 min. For depositing the buffer layer, a 0.5 mg ml<sup>-1</sup> bathocuproine solution (in isopropanol) is spin-coated at 5000 rpm for 30 s. Lastly, Ag is evaporated as top electrode with 80 nm thickness.

**DFT Calculation:** First-principles calculations were carried out using density functional theory (DFT) within the VASP code<sup>1,2</sup>. The frozen-core projected augmented wave approach<sup>3</sup> was employed to account for electron and core interactions. For structure relaxation and formation energy calculations, we employed the Perdew–Burke–Ernzerhof (PBE) functional<sup>4</sup>. To enhance the accuracy of our bandgap evaluations, we also performed calculations using the Heyd-Scuseria-Ernzerhof (HSE) functional<sup>5</sup> with  $\alpha = 0.25$ . The kinetic energy cutoff for the plane-wave basis functions was set to 400 eV, and all atoms are relaxed until the forces on each atom fall below 0.02 eV/Å. Brillouin zone integration was performed using k-point meshes with grid spacings of  $2\pi \times 0.025 \text{ \AA}^{-1}$  or smaller.

**Thin films and devices characterizations:** Scanning electron microscopy (SEM) and energy dispersive X-ray spectroscopy (SEM-EDS) characterizations were performed using FESEM (FESEM, JOEL, JSM-7600F). Transmission electron microscopy (TEM) and STEM-EDS was conducted on a JEOL 2100F at 200 kV. The TEM sample was a focussed ion beam (FIB) lamella prepared using a Zeiss Crossbeam 540. X-ray diffraction (XRD) patterns were collected on Bruker D8 Advance with Cu K $\alpha$  (1.5406 Å) as the source. The transmittance of the films was measured on Shimadzu UV-3600. As for the high throughput characterization, the transmittance was measured using customized Avantes AvaLight-DH-S-BAL and SensLine with automated XZ motor. The average visible transmittance (AVT) is measured from 380-780 nm. The substrate is vertically mounted on a bracket with x-z control. A light source and detector are positioned on either side of the substrate. The sheet resistance of the films was measured using a 4-point probe setup (Jandel RM3000+ unit) to ensure accuracy and repeatability. Measurements were conducted at five different locations across each sample to account for any inhomogeneity, and the average values were reported. Atomic force microscopy (AFM) images were acquired using a Bruker Dimension Icon microscope with a Nanoscope 6 controller in tapping mode. Images were obtained using ScanAsyst in air with a scan area of 1 μm × 1 μm with an SCM-PIT-V2 probe (Bruker). Nanoscope Analysis software (Bruker) was used for image processing, and *plane fit* correction was applied to eliminate sample tilting effects. X-ray photoelectron spectroscopy (XPS) measurement was conducted on an AXIS Supra spectrometer (Kratos Analytical) equipped with a monochromatic Al K $\alpha$  source (1487 eV). Ultraviolet photoelectron spectroscopy (UPS) was carried out on the same

instrument with a He(I) source (21.22 eV). AC Hall measurements were done on parallel dipole line AC Hall setup.<sup>6,7</sup> The current–voltage (I–V) curves were measured using a Keithley 2612A and a Xe-lamp-based solar simulator using AM1.5G spectrum.

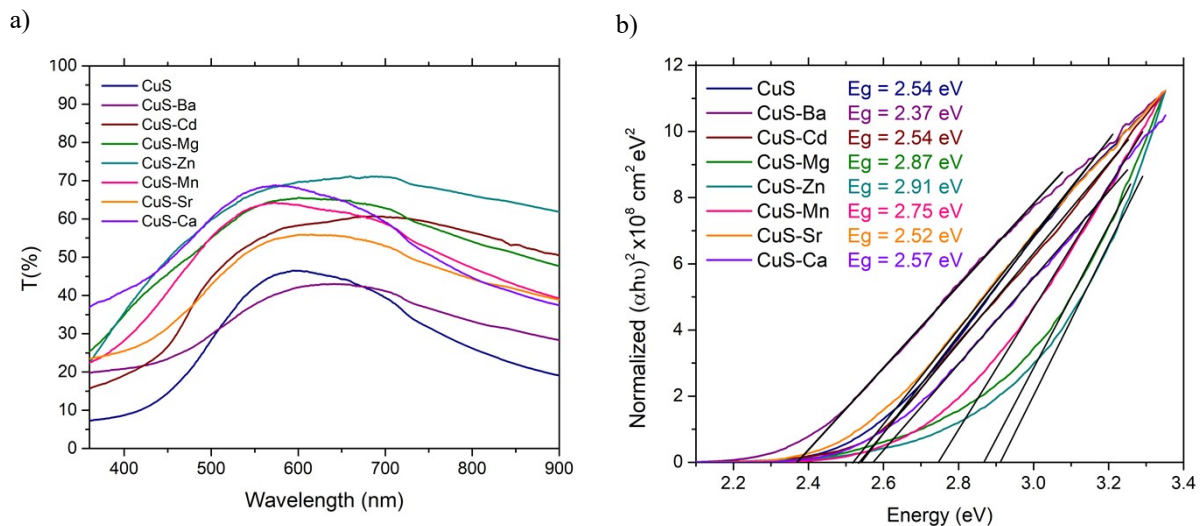


**Fig. S2.** (a) Transmittance spectra of CuS with addition of various cations and (b) the respective Tauc plots.

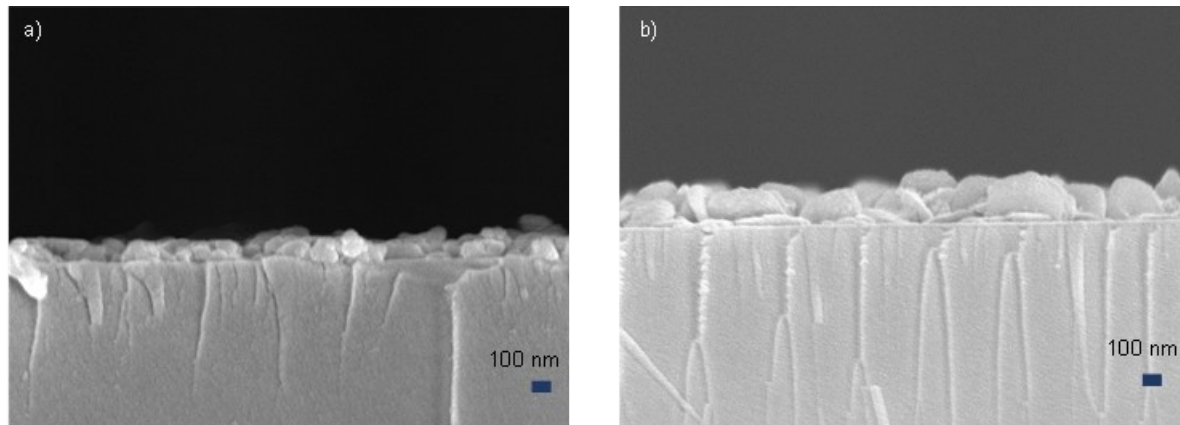


**Fig. S3.** Cross section SEM of CuS with (a) 2.5 mM concentration ( $\approx 100$  nm thickness) and (b) 12.5 mM concentration ( $\approx 300$  nm thickness)

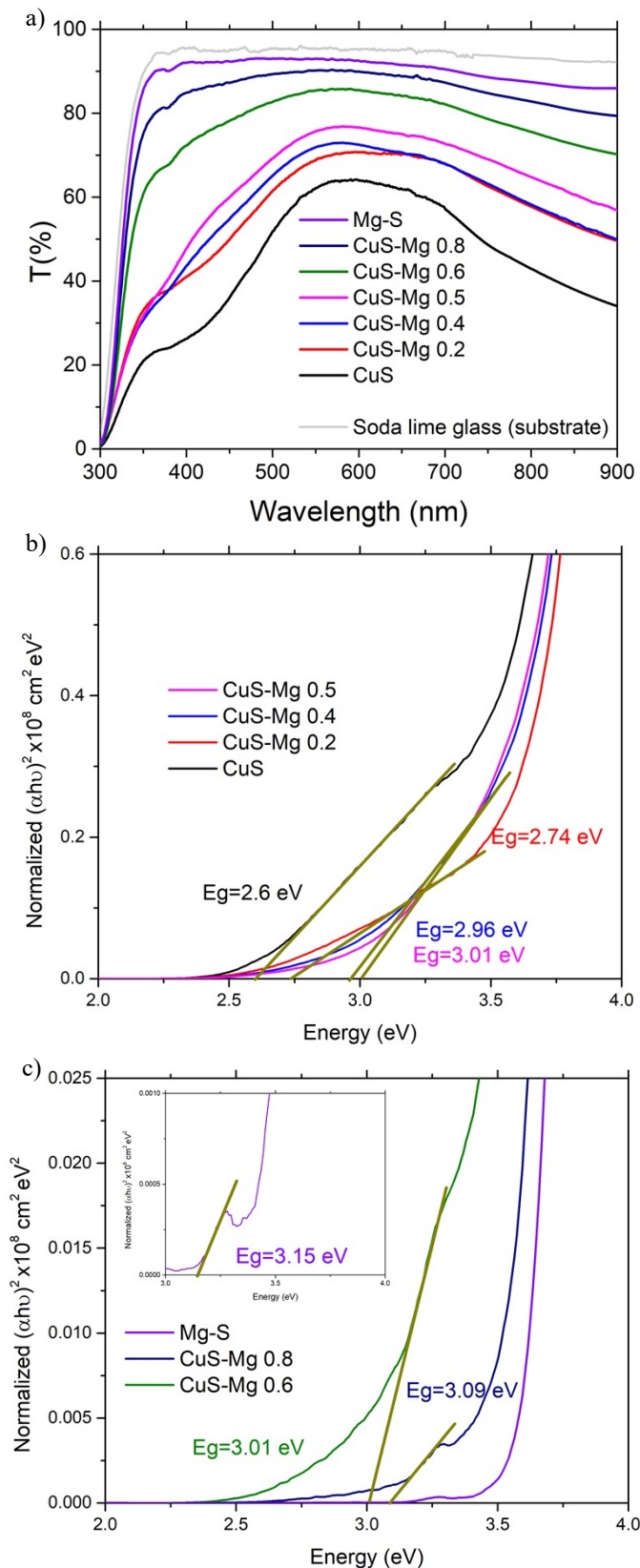


**Fig. S4.** (a) Transmittance spectra of CuS with different amount of Mg precursor. Tauc plots of (b) CuS, CuS-Mg 0.2, CuS-Mg 0.4, CuS-Mg 0.5 (c) CuS-Mg 0.6, CuS-Mg 0.8 and Mg-S.

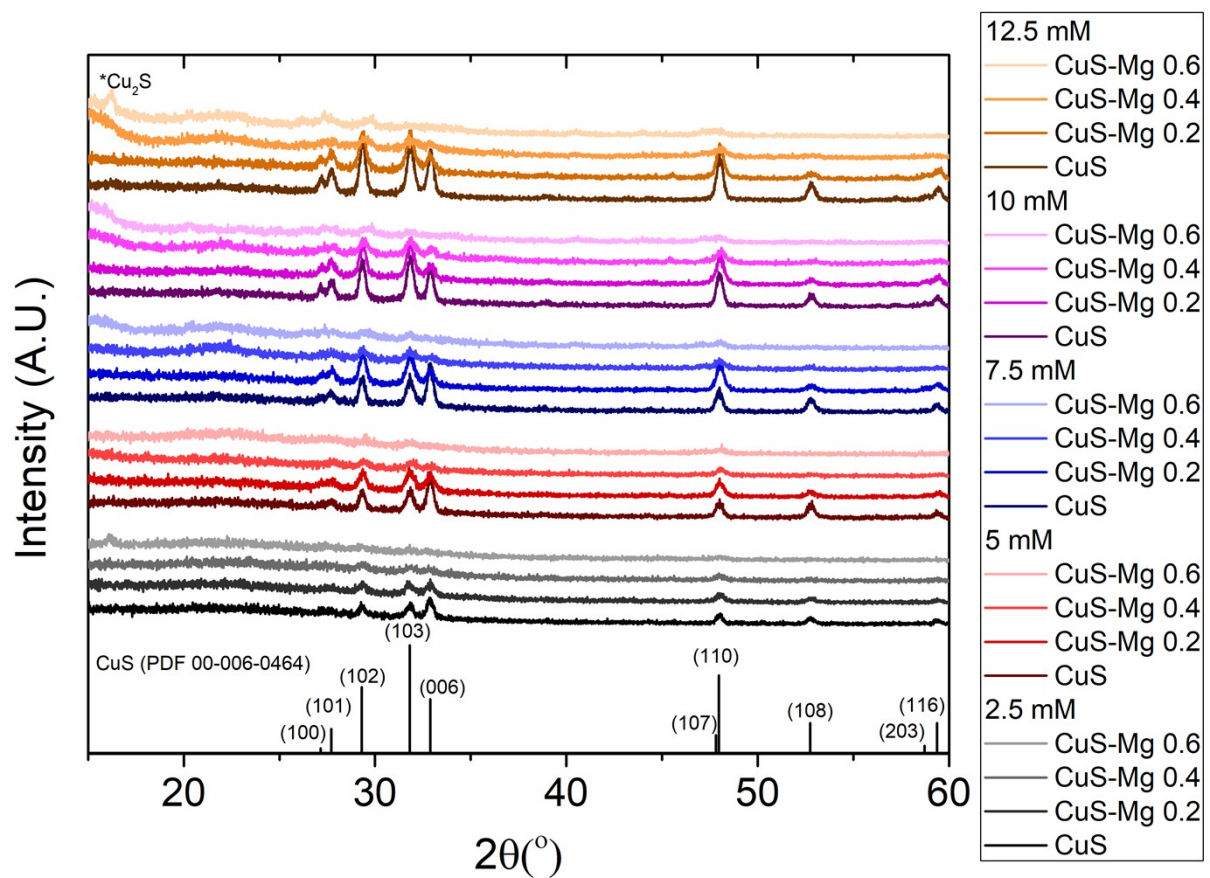


**Fig. S5.** XRD spectra of CuS with addition of Mg and different molarity.

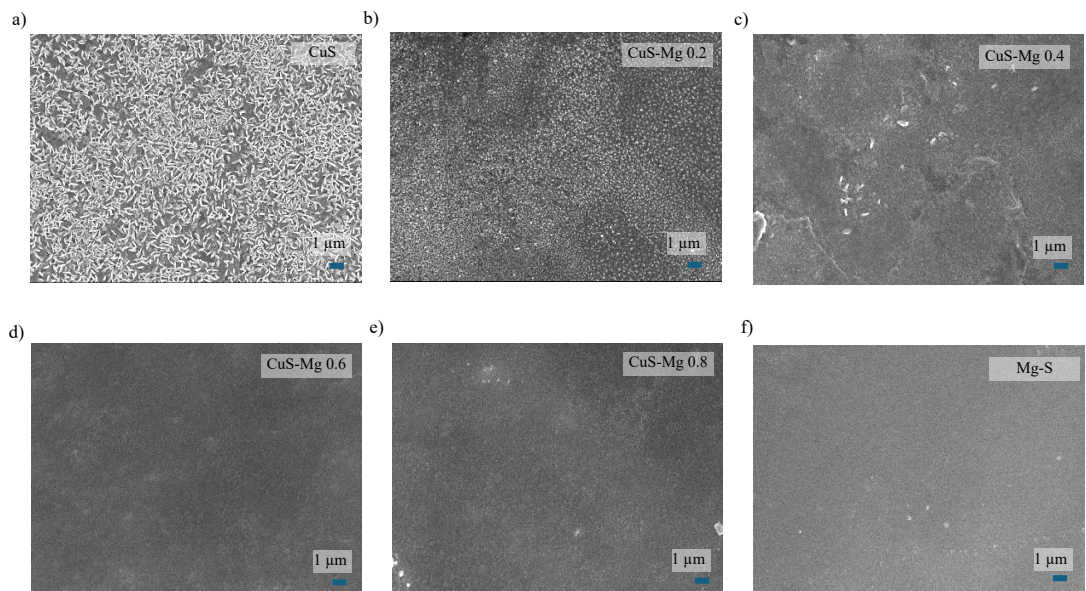


**Fig. S6.** Plan-view SEM images of (a) CuS, (b) CuS-Mg 0.2, (c) CuS-Mg 0.4, (d) CuS-Mg 0.6, (e) CuS-Mg 0.8 and (f) Mg-S.

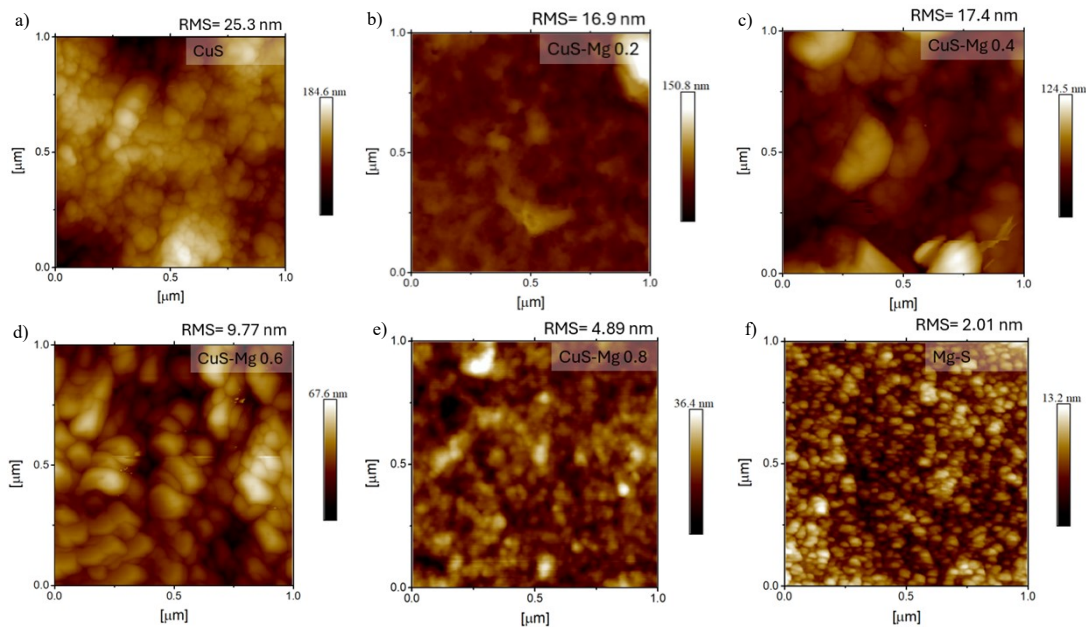


**Fig. S7.** AFM images and root-mean-square (RMS) roughness value of (a) CuS, (b) CuS-Mg 0.2, (c) CuS-Mg 0.4, (d) CuS-Mg 0.6, (e) CuS-Mg 0.8 and (f) Mg-S.

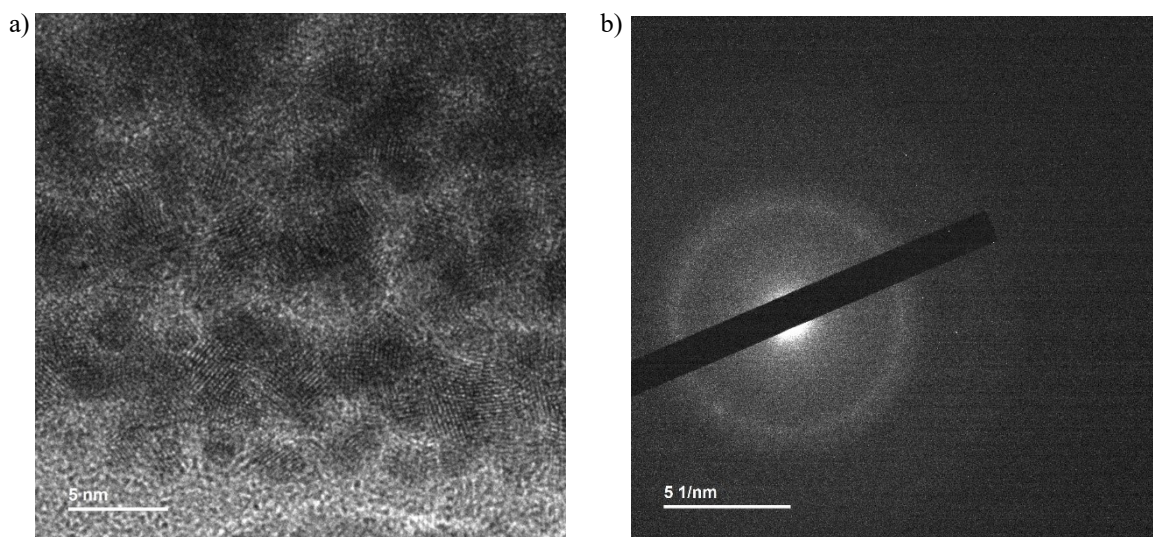


**Fig. S8.** (a) TEM image and (b) diffraction pattern of CuS-Mg 0.4.

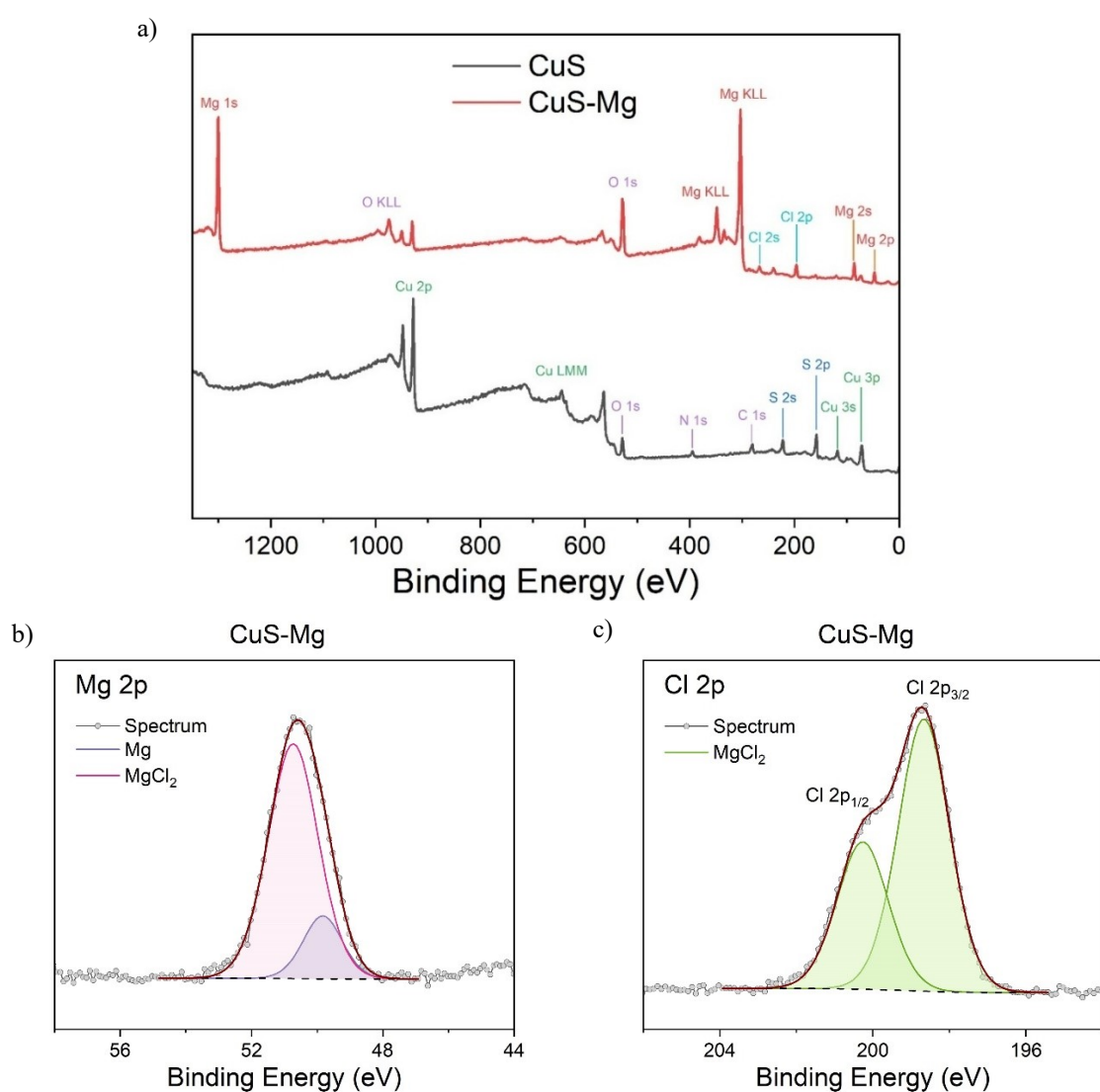
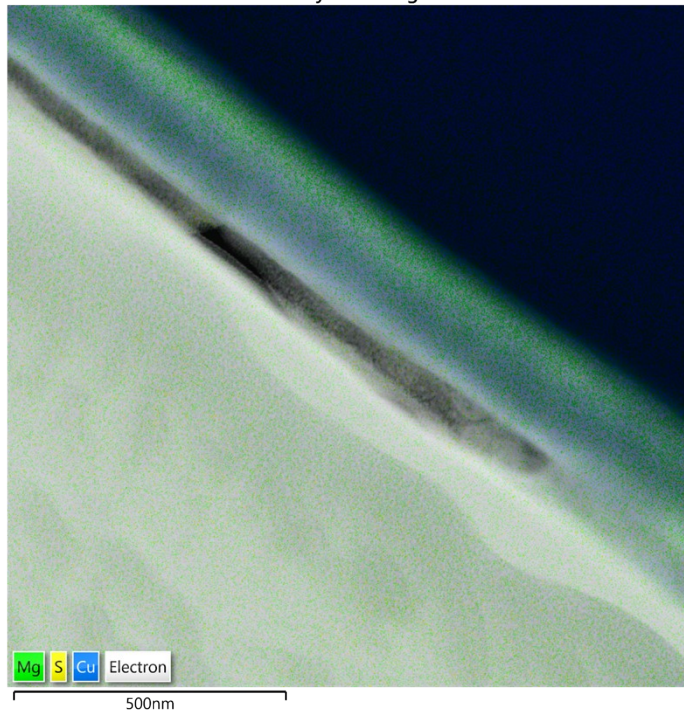
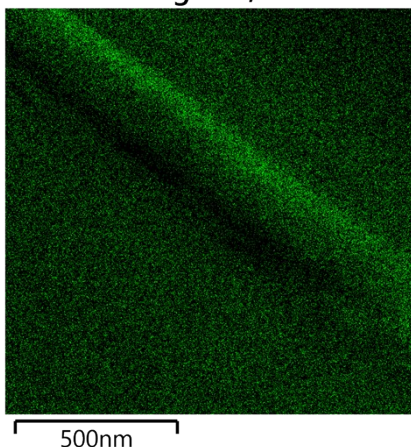


**Fig. S9.** (a) Wide XPS spectrum for CuS and CuS-Mg. XPS spectra of (b) Mg 2p and (c) Cl 2p on CuS-Mg film.

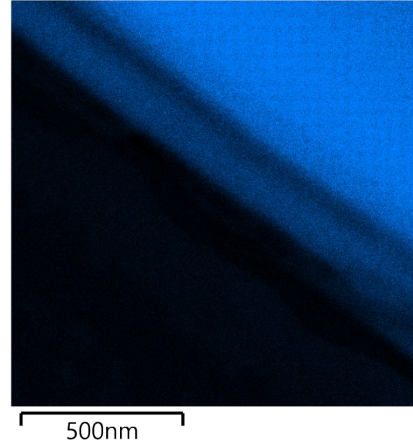
EDS Layered Image 1



Mg K $\alpha$ 1,2



Cu K $\alpha$ 1



S L $I$

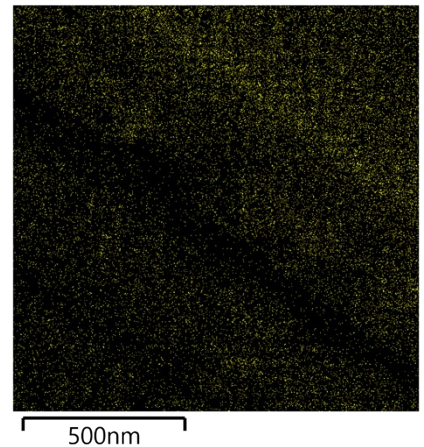


**Fig. S10.** STEM-EDS of CuS-Mg 0.4.

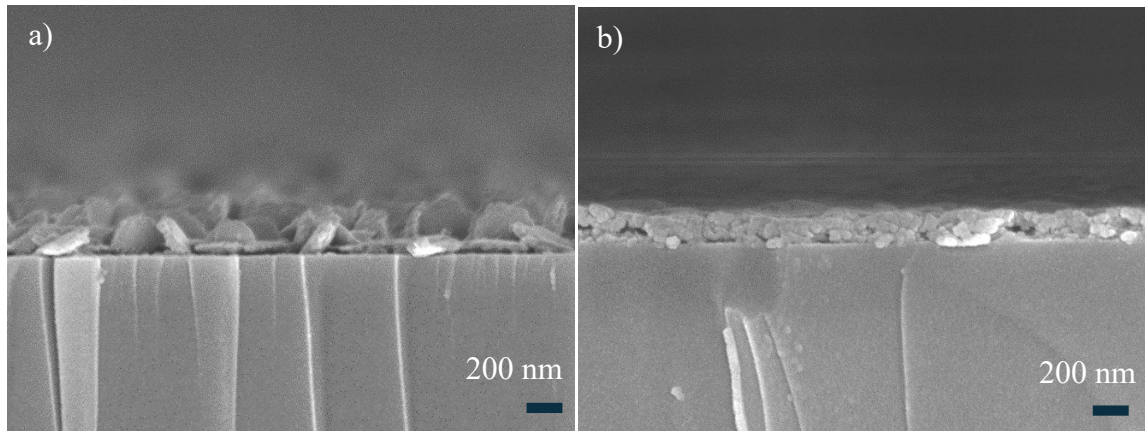


**Fig. S11.** Cross-section SEM of (a) CuS and (b) CuS-Mg.

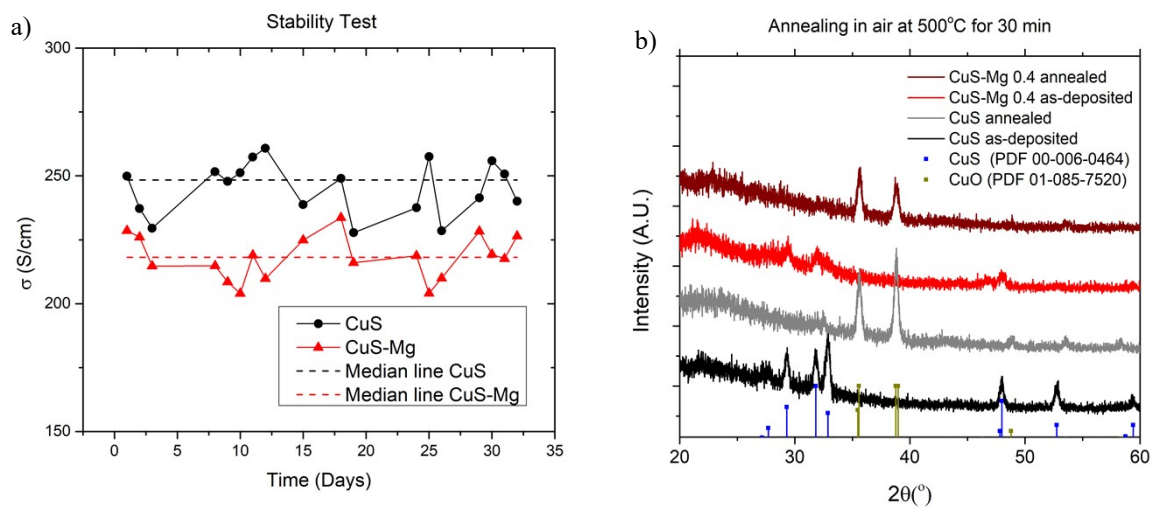


**Fig. S12.** (a) Stability test on electrical properties of CuS and CuS-Mg. (b) XRD spectra of CuS and CuS-Mg before and after annealing in air at 500°C for 30 minutes.

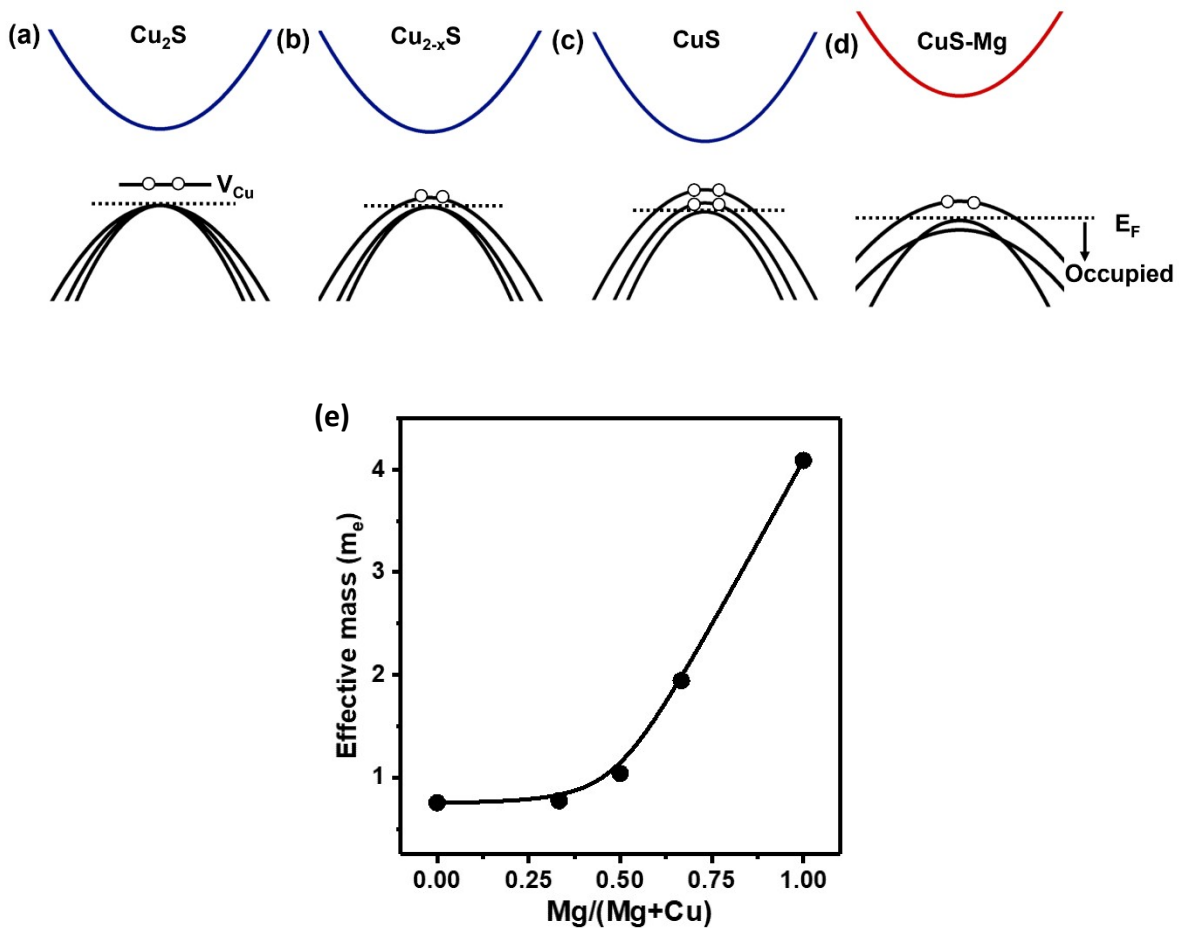


**Fig. S13.** Schematic of the evolution of p-type conductivity mechanism from (a) Cu<sub>2</sub>S to (b) Cu<sub>2-x</sub>S, (c) CuS, and (d) CuS-Mg. (e) DFT-calculated hole effective mass as a function of Mg/(Mg+Cu) ratio in the region of 0 to 1.

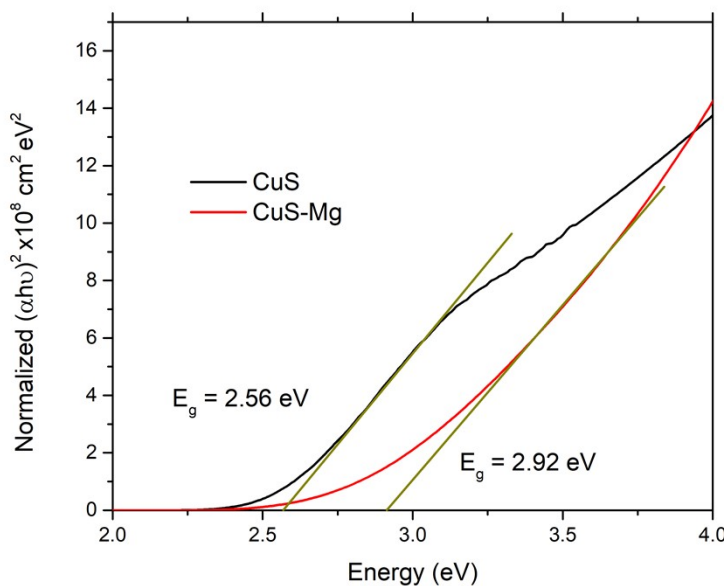


**Fig. S14.** Tauc plot of CuS and CuS-Mg based on direct transition ( $r = 1/2$ ).

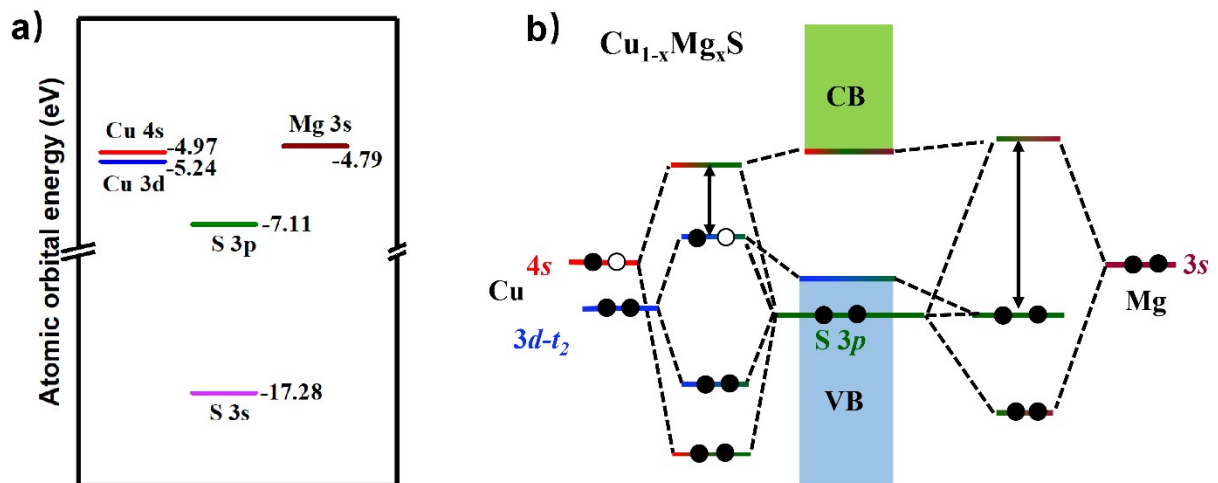


**Fig. S15.** (a) Atomic orbital energies: Cu (3d and 4s), Mg (3s), and S (3s and 3p). (b) Schematic representation of orbital interactions for the formation of VBM and CBM in  $\text{Cu}_{1-x}\text{Mg}_x\text{S}$  ( $0 < x < 1$ ).

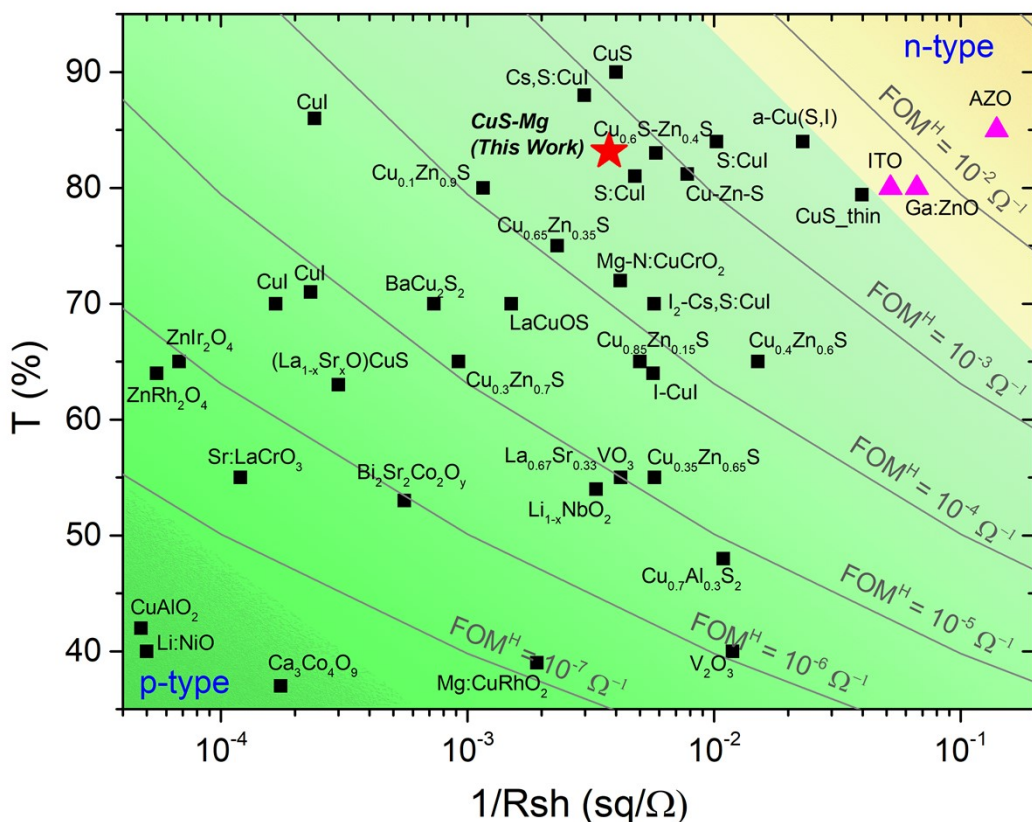


**Fig. S16.** List of different p-type transparent conducting materials as a function of transmittance at 550 nm and reciprocal of sheet resistance. The yellow area indicates the region of reported n-type transparent conducting oxides. The grey line indicated  $FOM^H$  values.

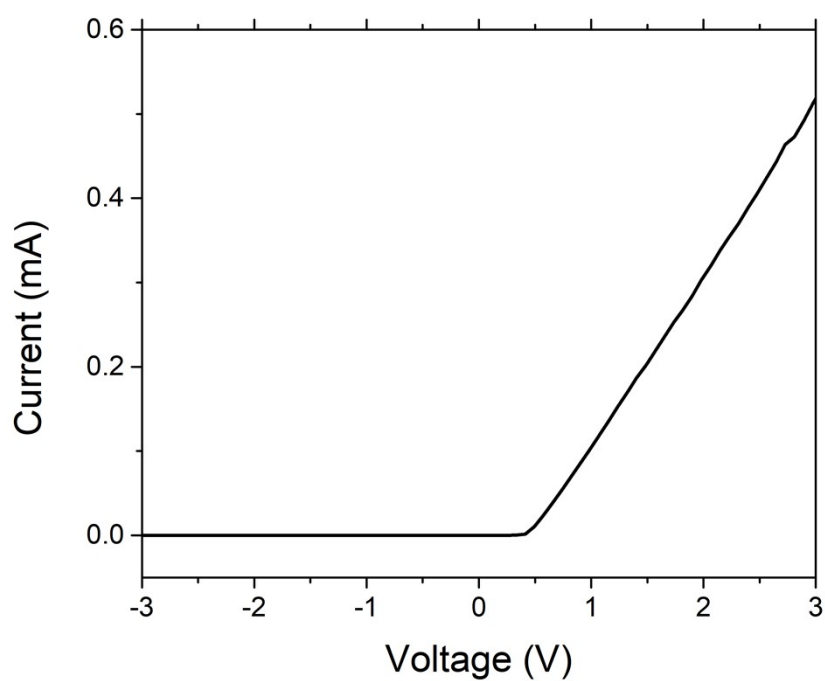


**Fig. S17.** Current-voltage measurement of CuS-Mg in linear coordinates.

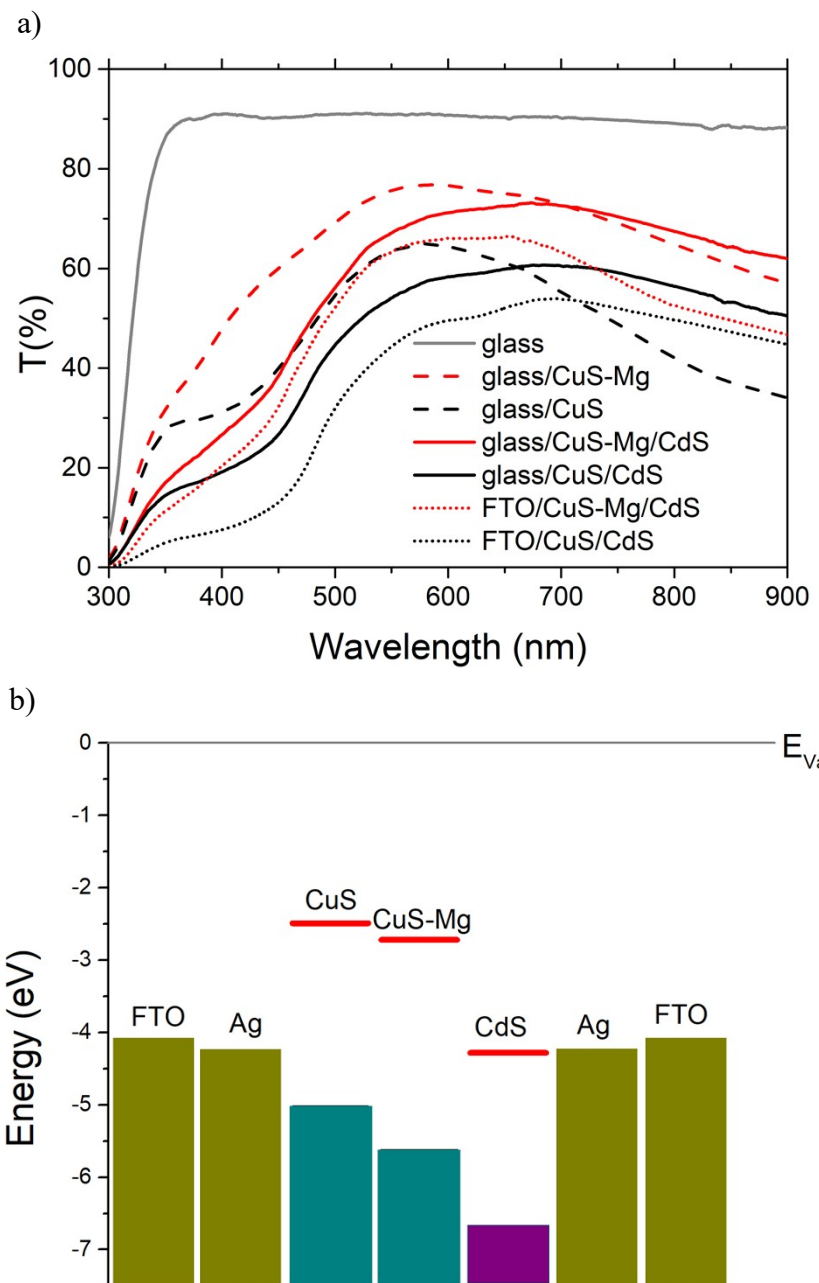


**Fig. S18.** (a) Transmittance of bare p-type TCMs, heterojunction stack with CdS and heterojunction with n-type TCMs. (b) Schematic of the band alignments for the various device stacks. CdS band alignment is based on previous study.<sup>8</sup>

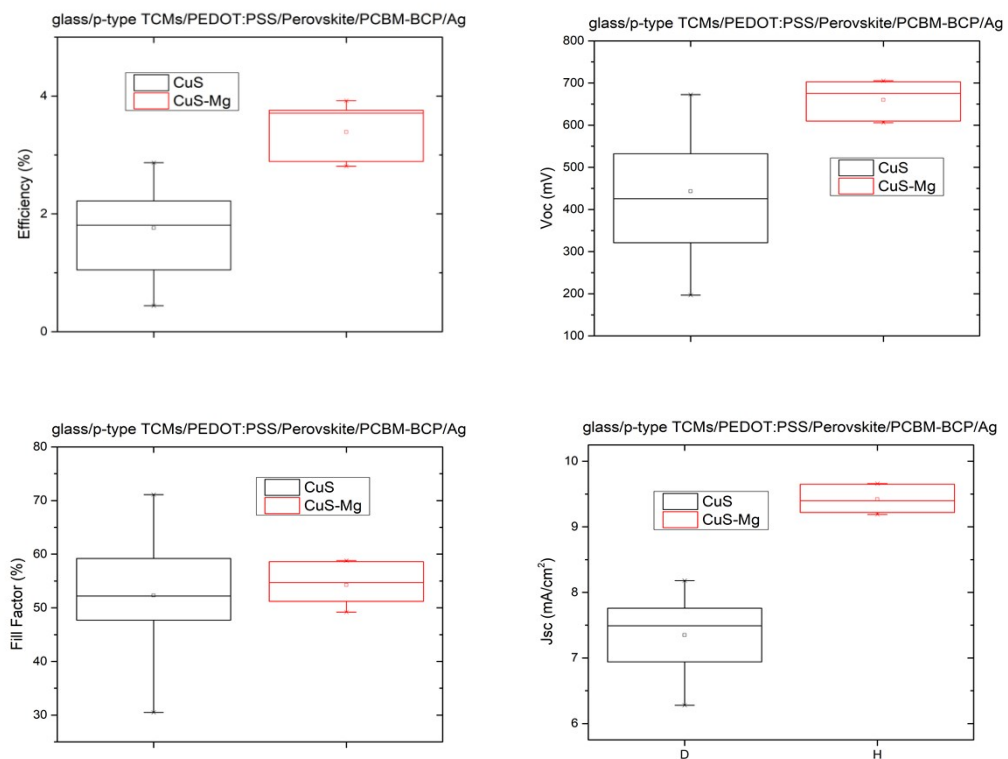


**Fig. S19.** Photovoltaic parameters (a) efficiency, (b) open circuit voltage ( $V_{oc}$ ), (c) fill factor and (d) short circuit current ( $J_{sc}$ ) of perovskite solar cell with CuS and CuS-Mg as bottom electrode.

**Table S1.** The optical and electrical property of CuS with different amount of Mg precursor. The concentration is kept at 0.005 M. Some data are derived from three samples from different batches.

	Average Rsh ( $\Omega/\square$ )	AVT (%)	Band gap (eV)	$\frac{T10}{FOM^H \cdot Rsh}$ ( $\times 10^{-6} \Omega^{-1}$ )	$\frac{1}{FOM^G \cdot Rsh \cdot \ln T}$ ( $\times 10^{-6} \Omega^{-1}$ )
CuS	$108.19 \pm 25.66$	$46.03 \pm 3.34$	2.60	$5.086 \pm 2.58$	$13046.04 \pm 2243.23$
CuS-Mg 0.2	$194.06 \pm 29.74$	$52.02 \pm 0.95$	2.74	$7.77 \pm 0.96$	$8267.31 \pm 1257.68$
CuS-Mg 0.4	$279.81 \pm 55.91$	$61.95 \pm 3.20$	2.96	$36.37 \pm 12.67$	$8057.94 \pm 1502.16$
CuS-Mg 0.5	$3098.44 \pm 1200.78$	$67.95 \pm 3.14$	3.01	$9.15 \pm 4.07$	$1055.22 \pm 291.75$
CuS-Mg 0.6	$28746.53 \pm 8067.45$	$73.58 \pm 3.77$	3.01	$3.05 \pm 2.21$	$153.49 \pm 68.89$
CuS-Mg 0.8	$5.80E+06 \pm 4.00E+06$	$75.07 \pm 6.64$	3.09	$0.54 \pm 0.52$	$42.75 \pm 42.17$
Mg-S	$1.95E+07 \pm 1.29E+07$	$74.95 \pm 8.36$	3.15	$0.01 \pm 2.00E-03$	$0.48 \pm 0.24$

**Table S2.** Binding energy (BE) of primary peak and corresponding atomic concentration for each chemical state

CuS				CuS-Mg			
Core level	BE (eV)	Chemical state	at.%	Core level	BE (eV)	Chemical state	at.%
Cu 2p <sub>3/2</sub>	932.3	CuS	54.22	Cu 2p <sub>3/2</sub>	932.2	CuS	33.48
	932.7	Cu <sub>2</sub> S	45.78		932.7	Cu <sub>2</sub> S	66.52
S 2p <sub>3/2</sub>	161.5	Cu <sub>2</sub> S	19.56	S 2p <sub>3/2</sub>	161.6	Cu <sub>2</sub> S	28.38
	162.4	CuS	43.38		162.7	CuS	9.87
	163.5	C-S-H/C-S-	37.06		163.3	C-S-H/C-S-	25.54

		C				C	
					168.8	C-SO <sub>3</sub> -H	36.30
				Mg 2p	49.8	Mg metal	17.33
					50.7	MgCl <sub>2</sub> /MgO	82.67
				Cl 2p <sub>3/2</sub>	198.7	MgCl <sub>2</sub>	100

**Table S3.** Chemical composition of CuS and Mg-modified CuS using SEM-EDS and XPS.

	Measurement	Atomic %				Mg/(Mg+Cu)	S/Cu
		Cu	S	Mg	Cl		
CuS	SEM-EDS	47.90	52.10	0.00	0.00	0.00	1.13
	XPS	45.57	54.43	0.00	0.00	0.00	1.19
CuS-Mg	SEM-EDS	24.79	25.75	39.50	9.96	0.61	1.04
	XPS	3.56	5.46	62.83	28.16	0.95	1.53

**Table S4.** The optoelectronic property of CuS and CuS-Mg before and after annealing under vacuum condition.

		Average Rsh ( $\Omega/\square$ )	AVT (%)	$FOM^H$	$FOM^G$
				$\frac{T^{10}}{Rsh}$	$\frac{1}{Rsh \cdot \ln T}$
As-deposited	CuS	74.63	41.13	1.85	15079.62
	CuS-Mg	276.30	65.94	56.28	8692.29
500°C annealing in vacuum for 30 min	CuS	687.32	45.86	0.60	1866.45
	CuS-Mg	338.53	63.90	33.53	6596.04

**Table S5.** Comparison of TCMs in literature

Materials	Thickness	Sheet Resistance	Conductivity, $\sigma$	Transmittance @	Absorption	$FOM^G$	$FOM^H$	Ref.
-----------	-----------	------------------	------------------------	-----------------	------------	---------	---------	------

	(nm)	nce, Rsh ( $\Omega/\square$ )	(S/cm)	550 nm, T (%)	Coeffien t, $\alpha$ @550nm $(\text{cm}^{-1})$	$\frac{1}{Rsh \cdot \ln T}$ ( $\times 10^{-6} \Omega^{-1}$ )	$\frac{T10}{Rsh}$ ( $\times 10^{-6} \Omega^{-1}$ )	
<b>P-type Transparent Conducting Materials</b>								
<i>Oxides</i>								
Cu <sub>2</sub> O	100	40000.0 0	2.50	55	59784	41.82	0.06	<sup>9</sup>
CuAlO <sub>2</sub>	500	21052.6 3	0.95	42	17350	54.76	0.01	<sup>10</sup>
CuScO <sub>2+x</sub>	110	6060.61	15.00	25	126027	119.02	1.57E- 04	<sup>11</sup>
CuGaO <sub>2</sub>	500	317460. 32	0.06	91	1886	33.40	1.23	<sup>12</sup>
CuY <sub>1-x</sub> Ca <sub>x</sub> O <sub>2</sub>	240	41666.6 7	1.00	50	28881	34.62	0.02	<sup>13</sup>
Mg:N-CuCrO <sub>2</sub>	150	239.81	278.00	72	21900	12693.9 1	156.12	<sup>14</sup>
Mg:CuRhO <sub>2</sub>	40	522.51	478.46	39	235402	2032.52	0.16	<sup>15</sup>
K:SrCu <sub>2</sub> O <sub>2</sub>	120	1.67E+0 6	0.05	85	13543	3.69	0.12	<sup>16</sup>
ZnRh <sub>2</sub> O <sub>4</sub>	200	18181.8 2	2.75	64	22314	123.24	0.63	<sup>17</sup>
ZnIr <sub>2</sub> O <sub>4</sub>	200	14749.2 6	3.39	65	21539	157.39	0.91	<sup>17</sup>
Bi <sub>2</sub> Sr <sub>2</sub> Co <sub>2</sub> O <sub>y</sub>	25	1801.80	222.00	53	253951	874.18	0.97	<sup>18</sup>
Ca <sub>3</sub> Co <sub>4</sub> O <sub>9</sub>	100	5714.29	17.50	37	99425	176.01	0.01	<sup>19</sup>
Sr:LaCrO <sub>3</sub>	80	8333.33	15.00	55	74730	200.72	0.30	<sup>20</sup>
Cr <sub>2</sub> O <sub>3</sub> :(Mg, N)	150	202020. 20	0.33	44	54732	6.03	1.35E- 03	<sup>21</sup>
Mg:AgCrO <sub>2</sub>	120	1.23E+0 6	0.07	56	48318	1.40	2.46E- 03	<sup>22</sup>
AgGaO <sub>2</sub>	180	1.74E+0	3.20E-04	47	41946	0.01	3.03E- 23	

		8					06	
AgCoO <sub>2</sub>	150	333333. 33	0.20	48	48931	4.09	1.95E- 03	<sup>24</sup>
K:Ba <sub>2</sub> BiTa O <sub>6</sub>	120	2.60E+0 8	3.20E-04	88	10653	0.03	1.07E- 03	<sup>25</sup>
V <sub>2</sub> O <sub>3</sub>	56	84.15	2122.00	40	163623	12968.8 1	1.25	<sup>26</sup>
La <sub>0.67</sub> Sr <sub>0.33</sub> VO <sub>3</sub>	48	238.83	872.30	55	124549	7003.65	10.61	<sup>27</sup>
Li:NiO	100	20000.0 0	5.00	40	91629	54.57	0.01	<sup>28</sup>
Li <sub>1-x</sub> NbO <sub>2</sub>	100	301.20	332.00	54	61619	5387.98	7.00	<sup>29</sup>
SnO	15	1.10E+0 7	0.06	95	34196	1.78	0.05	<sup>30</sup>
<b><i>Sulfides</i></b>								
CuS nanosheet	10	25.13	39800.00	79	230672	172539. 50	3963.5 8	<sup>31</sup>
CuS	40	250.00	1000.00	90	26340	37964.8 9	1394.7 1	<sup>32</sup>
Cu-Zn-S	52	128.35	1498.33	81	40049	37412.3 9	970.89	<sup>33</sup>
Cu <sub>0.85</sub> Zn <sub>0.15</sub> S	50	200.00	1000.00	65	86157	11606.7 7	67.31	<sup>34</sup>
Cu <sub>0.65</sub> Zn <sub>0.35</sub> S	50	431.97	463.00	75	57536	8047.08	130.37	<sup>34</sup>
Cu <sub>0.6</sub> S- Zn <sub>0.4</sub> S	60	171.82	970.00	83	31055	31234.9 8	903.03	<sup>35</sup>
Cu <sub>0.4</sub> Zn <sub>0.6</sub> S	200	66.50	751.88	65	21539	34907.6 1	202.45	<sup>36</sup>
Cu <sub>0.35</sub> Zn <sub>0.65</sub> S	220	174.09	261.10	55	27174	9608.30	14.55	<sup>37</sup>
Cu <sub>0.3</sub> Zn <sub>0.7</sub> S	218	1087.00	42.20	65	19761	2135.55	12.39	<sup>38</sup>
Cu <sub>0.1x</sub> Zn <sub>0.9</sub> S	220	863.83	52.62	80	10143	5187.87	124.30	<sup>37</sup>
Cu <sub>0.7</sub> Al <sub>0.3</sub> S <sub>2</sub>	200	91.58	546.00	48	36698	14878.0 1	7.09	<sup>39</sup>

BaCu <sub>2</sub> S <sub>2</sub>	430	1367.99	17.00	70	8295	2049.49	20.65	<sup>40</sup>
CuS	260	153.36	250.79	68	14692	17069.9 7	142.99	This wor k
CuS-Mg	164	266.29	228.98	83	11251	20351.3 1	593.29	This wor k
<b>Halides</b>								
CuI – Thermal Evaporatio n	120	5999.52	13.89	70	29723	467.32	4.71	<sup>41</sup>
CuI – Solid Iodination	70	4329.00	33.00	71	48927	674.47	7.52	<sup>42</sup>
CuI - Sputtering	240	4166.67	10.00	86	6284	1591.27	53.11	<sup>43</sup>
I doped- CuI	200	176.68	283.00	64	22314	12682.4 2	65.26	<sup>44</sup>
a-Cu(S,I)	100	43.72	2287.50	84	17435	131199. 06	4000.8 7	<sup>45</sup>
S:CuI	200	97.85	511.00	84	8718	58616.5 8	1787.4 9	<sup>46</sup>
S:CuI (3% at. S)	110	209.08	434.80	81	19156	22697.3 1	581.48	<sup>47</sup>
Cs,S:CuI	100	335.68	297.90	88	13000	22400.0 0	829.65	<sup>48</sup>
I <sub>2</sub> -Cs,S:CuI	100	174.64	572.60	70	36800	15600.0 0	161.75	<sup>48</sup>
<b>Others</b>								
LacCuOS	110	665.03	136.70	70	32425	4215.88	42.48	<sup>49</sup>
(La <sub>1-x</sub> Sr <sub>x</sub> O) CuS	150	3333.33	20.00	63	30802	649.30	2.95	<sup>50</sup>
BP	116	41050.9 0	2.10	45	68837	36.00	0.01	<sup>51</sup>
<b>N-type Transparent Conducting Materials</b>								
Al:ZnO	700	7	2000	85	2322	861438	27562	<sup>52</sup>

(AZO)								
Sn:In <sub>2</sub> O <sub>3</sub> (ITO)	200	19	2600	80	11157	233034	5583	<sup>53</sup>
Ga:ZnO	350	15	1900	80	6376	298014	7140	<sup>54</sup>

## References

1. G. Kresse and J. Furthmüller, *Physical Review B*, 1996, **54**, 11169-11186.
2. G. Kresse and J. Furthmüller, *Computational Materials Science*, 1996, **6**, 15-50.
3. G. Kresse and D. Joubert, *Physical review b*, 1999, **59**, 1758.
4. J. P. Perdew, K. Burke and M. Ernzerhof, *Physical Review Letters*, 1996, **77**, 3865-3868.
5. J. Paier, M. Marsman, K. Hummer, G. Kresse, I. C. Gerber and J. G. Ángyán, *The Journal of Chemical Physics*, 2006, **124**.
6. "Hall Measurement System with Rotary Magnet", US Patent 9,041,389, "Rotating magnetic Field Hall measurement system", US Patent App.14/682696, 14/748495, 2014.
7. O. Gunawan, Y. Virgus and K. F. Tai, *Applied Physics Letters*, 2015, **106**, 062407.
8. A. Klein, *Journal of physics: Condensed matter*, 2015, **27**, 134201.
9. A. Sekkat, M. O. Liedke, V. H. Nguyen, M. Butterling, F. Baiutti, J. d. D. Sirvent Veru, M. Weber, L. Rapenne, D. Bellet and G. Chichignoud, *Nature Communications*, 2022, **13**, 5322.
10. H. Kawazoe, M. Yasukawa, H. Hyodo, M. Kurita, H. Yanagi and H. Hosono, *Nature*, 1997, **389**, 939-942.
11. N. Duan, A. Sleight, M. Jayaraj and J. Tate, *Applied Physics Letters*, 2000, **77**, 1325-1326.
12. K. Ueda, T. Hase, H. Yanagi, H. Kawazoe, H. Hosono, H. Ohta, M. Orita and M. Hirano, *Journal of Applied Physics*, 2001, **89**, 1790-1793.
13. M. Jayaraj, A. Draeseke, J. Tate and A. Sleight, *Thin solid films*, 2001, **397**, 244-248.
14. M. Ahmadi, M. Asemi and M. Ghanaatshoar, *Applied Physics Letters*, 2018, **113**.
15. C. Li, P. Gong, J. Zheng, M. Zhao, R. Wei, W. Cheng, L. Hu, W. Song, X. Zhu and Y. Sun, *Advanced Optical Materials*, 2022, **10**, 2102559.
16. A. Kudo, H. Yanagi, H. Hosono and H. Kawazoe, *Applied Physics Letters*, 1998, **73**, 220-222.
17. M. Dekkers, G. Rijnders and D. H. Blank, *Applied physics letters*, 2007, **90**.
18. R. Wei, X. Tang, L. Hu, Z. Hui, J. Yang, H. Luo, X. Luo, J. Dai, W. Song and Z. Yang, *Chemical Communications*, 2014, **50**, 9697-9699.
19. M. Aksit, S. Kolli, I. Slauch and R. D. Robinson, *Applied Physics Letters*, 2014, **104**.
20. K. H. Zhang, Y. Du, A. Papadogianni, O. Bierwagen, S. Sallis, L. F. Piper, M. E. Bowden, V. Shuththanandan, P. V. Sushko and S. A. Chambers, *Advanced Materials*, 2015, **27**, 5191-5195.
21. E. Arca, K. Fleischer and I. Shvets, *Applied Physics Letters*, 2011, **99**.
22. R. Wei, X. Tang, L. Hu, J. Yang, X. Zhu, W. Song, J. Dai, X. Zhu and Y. Sun, *Journal of Materials Chemistry C*, 2017, **5**, 1885-1892.
23. K. Vanaja, R. Ajimsha, A. Asha and M. Jayaraj, *Applied physics letters*, 2006, **88**.
24. J. Tate, M. Jayaraj, A. Draeseke, T. Ulbrich, A. Sleight, K. Vanaja, R. Nagarajan, J. F. Wager and R. Hoffman, *Thin solid films*, 2002, **411**, 119-124.

25. A. Bhatia, G. Hautier, T. Nilgianskul, A. Miglio, J. Sun, H. J. Kim, K. H. Kim, S. Chen, G.-M. Rignanese and X. Gonze, *Chemistry of Materials*, 2016, **28**, 30-34.
26. L. Hu, M. Zhao, S. Liang, D. Song, R. Wei, X. Tang, W. Song, J. Dai, G. He and C. Zhang, *Physical Review Applied*, 2019, **12**, 044035.
27. L. Hu, R. Wei, J. Yan, D. Wang, X. Tang, X. Luo, W. Song, J. Dai, X. Zhu, C. Zhang and Y. Sun, *Advanced Electronic Materials*, 2018, **4**, 1700476.
28. K. O. Egbo, C. E. Ekuma, C. P. Liu and K. M. Yu, *Physical Review Materials*, 2020, **4**, 104603.
29. T. Soma, K. Yoshimatsu and A. Ohtomo, *Science Advances*, 2020, **6**, eabb8570.
30. J. A. Caraveo-Frescas, P. K. Nayak, H. A. Al-Jawhari, D. B. Granato, U. Schwingenschlogl and H. N. Alshareef, *ACS nano*, 2013, **7**, 5160-5167.
31. J. Hong, B.-S. Kim, B. Hou, S. Pak, T. Kim, A.-R. Jang, Y. Cho, S. Lee, G.-H. An and J. E. Jang, *ACS Applied Materials & Interfaces*, 2021, **13**, 4244-4252.
32. S. S. Pathak and L. S. Panchakarla, *Applied Materials Today*, 2021, **24**, 101152.
33. E. Jose, M. Mohan, M. A. G. Namboothiry and M. C. S. Kumar, *Journal of Alloys and Compounds*, 2020, **829**, 154507.
34. X. Xu, J. Bullock, L. T. Schelhas, E. Z. Stutz, J. J. Fonseca, M. Hettick, V. L. Pool, K. F. Tai, M. F. Toney, X. Fang, A. Javey, L. H. Wong and J. W. Ager, *Nano Lett*, 2016, **16**, 1925-1932.
35. A. Mallick, S. Chattopadhyay, G. De and D. Basak, *Journal of Alloys and Compounds*, 2019, **770**, 813-822.
36. S. K. Maurya, Y. Liu, X. Xu, R. Woods-Robinson, C. Das, J. W. Ager and K. Balasubramaniam, *Journal of Physics D: Applied Physics*, 2017, **50**, 505107.
37. M. Feng, H. Zhou, W. Guo, D. Zhang, L. Ye, W. Li, J. Ma, G. Wang and S. Chen, *Journal of Alloys and Compounds*, 2018, **750**, 750-756.
38. R. Woods-Robinson, J. K. Cooper, X. Xu, L. T. Schelhas, V. L. Pool, A. Faghaninia, C. S. Lo, M. F. Toney, I. D. Sharp and J. W. Ager III, *Advanced Electronic Materials*, 2016, **2**, 1500396.
39. X. Dai, H. Lei, C. Chen, Y. Guo and G. Fang, *RSC advances*, 2018, **8**, 16887-16896.
40. S. Park, D. A. Keszler, M. M. Valencia, R. L. Hoffman, J. P. Bender and J. F. Wager, *Applied physics letters*, 2002, **80**, 4393-4394.
41. D. K. Kaushik, M. Selvaraj, S. Ramu and A. Subrahmanyam, *Solar Energy Materials and Solar Cells*, 2017, **165**, 52-58.
42. N. Yamada, R. Ino and Y. Ninomiya, *Chemistry of Materials*, 2016, **28**, 4971-4981.
43. P. Storm, M. Bar, G. Benndorf, S. Selle, C. Yang, H. Von Wenckstern, M. Grundmann and M. Lorenz, *APL Materials*, 2020, **8**.
44. C. Yang, M. Kneiß, M. Lorenz and M. Grundmann, *Proceedings of the National Academy of Sciences*, 2016, **113**, 12929-12933.
45. F. Geng, Y.-N. Wu, D. Splith, L. Wang, X. Kang, X. Chen, P. Guo, S. Liang, L. Yang and M. Lorenz, *The Journal of Physical Chemistry Letters*, 2023, **14**, 6163-6169.
46. K. Ahn, G. H. Kim, S.-J. Kim, J. Kim, G.-S. Ryu, P. Lee, B. Ryu, J. Y. Cho, Y.-H. Kim and J. Kang, *Chemistry of Materials*, 2022, **34**, 10517-10527.
47. A. S. Mirza, M. Pols, W. Soltanpoor, S. Tao, G. Brocks and M. Morales-Masis, *Matter*, 2023.
48. A. S. Mirza, B. Vishal, P. Dally, C. S. Schnohr, S. De Wolf and M. Morales-Masis, *Advanced Functional Materials*, 2024, **34**, 2316144.
49. G. Gao, K. Li, L. Yang, F. Xia, L. Xu, J. Han, H. Gong and J. Zhu, *Materials Today Physics*, 2023, 101089.
50. H. Hiramatsu, K. Ueda, H. Ohta, M. Orita, M. Hirano and H. Hosono, *Thin Solid Films*, 2002, **411**, 125-128.

51. A. Crovetto, J. M. Adamczyk, R. R. Schnepf, C. L. Perkins, H. Hempel, S. R. Bauers, E. S. Toberer, A. C. Tamboli, T. Unold and A. Zakutayev, *Advanced Materials Interfaces*, 2022, **9**, 2200031.
52. K. Matsubara, P. Fons, K. Iwata, A. Yamada and S. Niki, *Thin Solid Films*, 2002, **422**, 176-179.
53. T. Ashida, A. Miyamura, N. Oka, Y. Sato, T. Yagi, N. Taketoshi, T. Baba and Y. Shigesato, *Journal of applied physics*, 2009, **105**.
54. E. Fortunato, A. Goncalves, V. Assuncao, A. Marques, H. Aguas, L. Pereira, I. Ferreira and R. Martins, *Thin solid films*, 2003, **442**, 121-126.